

Quantum Fisher information in quantum critical systems with topological characterizationShaoying Yin,^{1,2} Jie Song,² Yujun Zhang,¹ and Shutian Liu^{2,*}¹*Department of Physics, Harbin University, Harbin 150086, China*²*Department of Physics, Harbin Institute of Technology, Harbin 150001, China* (Received 25 July 2019; revised manuscript received 4 November 2019; published 21 November 2019)

We study the relationship between the quantum Fisher information (QFI) of spin pairs and the topological quantum phase transitions (TQPTs) of the extended XY model driven by the anisotropies of the nearest-neighbor and the next-nearest-neighbor spins, the transverse magnetic field, and the three-spin interaction. We find that the first derivative of QFI can correctly characterize the TQPTs at absolute zero temperature. Meanwhile, the impacts of the thermal fluctuations and the site distance of spin pairs on the critical behaviors of the QFI are studied. It is found that the first derivative of QFI for the nearest neighbor or the long-distance spin pairs can only correctly characterize the critical points of the TQPTs at sufficiently low temperature. Remarkably, when the anisotropy of the nearest-neighbor and the next-nearest-neighbor spins are the driven parameters and the site distance $R = 5$, the QFI itself can characterize the TQPTs at absolute zero temperature.

DOI: [10.1103/PhysRevB.100.184417](https://doi.org/10.1103/PhysRevB.100.184417)**I. INTRODUCTION**

Recently, topological quantum phases [1] in various systems have become of great significance due to their potential importance in both condensed matter physics [2–4] and quantum information science [5–8]. A quantum system with different topological quantum phases will possess different physical properties, which is important to study the physical properties of some magnetic materials. Thus, topological quantum phase transitions (TQPTs) have become one of the hottest research topics in condensed matter physics. The TQPTs cannot be described by the symmetry-breaking theory of Landau, and be characterized by the topological quantum discrete numbers [9,10]. A detailed study on TQPTs not only supplements the theory of quantum phase transitions, but also deepens our understanding of topological quantum phases from the standpoint of quantum mechanics. People have done extensive research on theoretical [9–14] and experimental [15,16] aspects.

A quantum many-body system represents an ideal platform for the investigation on the TQPTs. The Kitaev chain and the extended Ising model, two prototypical many-body models, are often used to investigate the TQPTs, including the theory of TQPTs [9–14,17–19] and the detection of TQPTs by several quantum concepts, such as quantum correlations [20–24], quantum coherence [25,26], and quantum deficit [27]. Quantum Fisher information (QFI) [28,29] is an extension of Fisher information [30] in the quantum realm, and is a fundamental concept of quantum metrology [31–34]. The QFI plays an important role in quantum detection and estimation because it can provide a bound about the accuracy of quantum estimation, i.e., a larger QFI means a higher estimation precision. The QFI, as a central quantity in quantum metrology, has been used to characterize the quantum phase

transitions (can be described by Landau symmetry-breaking theory) in various spin-chain systems recently [35–38]. In these works, there is only one or two phase transition points in various spin systems without topological characterizations. However, the TQPTs, beyond the symmetry-breaking theory of Landau, are characterized by the topological order, and are entirely different from the conventional quantum phase transitions. Second, the extended XY model in our work is rich in topological quantum phases, and is sensitive to many physical parameters at sufficiently low temperature, such as the anisotropies of the nearest-neighbor and the next-nearest-neighbor spins, the transverse magnetic field, and the three-spin interaction. Consequently, it is worth investigating the relationship between the QFI of spin pairs and the TQPTs in an extended XY spin chain.

In this work we investigate in detail the QFI of spin pairs and the critical behavior of its first derivatives in an extended XY spin chain. The research results show that the first derivative of the QFI (i.e., its first derivative is divergent at TQPTs points) can correctly mark the TQPTs driven by the anisotropies of the nearest-neighbor and the next-nearest-neighbor spins, the transverse magnetic field, and the three-spin interaction at absolute zero temperature. However, the impact of thermal fluctuations cannot be neglected to study the corresponding relation between the first derivative of the QFI and TQPTs in a many-body system. We also find that the first derivative of QFI for long-distance spin pairs can still mark the TQPTs in the extended XY model.

The paper is organized as follows. In Sec. II we give an overview of the extended XY model, and analyze its topological characterizations. The general expressions of the QFI are also introduced. In Sec. III we investigate the relationship between the QFI of spin pairs and the TQPTs of the extended XY chain driven by four physical parameters, and analyze the impact of thermal fluctuations and site distance of spin pairs on the critical behaviors of the QFI. The conclusion is given in Sec. IV.

*stliu@hit.edu.cn

II. PHYSICAL MODEL AND QUANTUM FISHER INFORMATION

A. Extended XY model and its topological characterizations

The physical model is a one-dimensional spin chain with topological characterizations, its Hamiltonian can be written as [11,12,25,27]

$$H = \sum_{i=1}^N \left[\left(\frac{1+\gamma}{2} \sigma_i^x \sigma_{i+1}^x + \frac{1-\gamma}{2} \sigma_i^y \sigma_{i+1}^y + \lambda \sigma_i^z \right) + \alpha \sigma_i^z \left(\frac{1+\delta}{2} \sigma_{i-1}^x \sigma_{i+1}^x + \frac{1-\delta}{2} \sigma_{i-1}^y \sigma_{i+1}^y \right) \right], \quad (1)$$

where γ and δ denote the anisotropies of the spin system arising from the nearest-neighbor and next-nearest-neighbor spins, respectively. λ represents the strength of the external magnetic field, and α is the strength of the three-spin interaction.

The reduced density matrix for the m th and n th sites can be written as

$$\rho_{mn} = \begin{pmatrix} u^+ & 0 & 0 & y^- \\ 0 & z & y^+ & 0 \\ 0 & y^+ & z & 0 \\ y^- & 0 & 0 & u^- \end{pmatrix}, \quad (2)$$

where $u^\pm = (1 \pm 2\langle \sigma^z \rangle + \langle \sigma_m^z \sigma_n^z \rangle)/4$, $y^\pm = (\langle \sigma_m^x \sigma_n^x \rangle \pm \langle \sigma_m^y \sigma_n^y \rangle)/4$, and $z = [1 - \langle \sigma_m^z \sigma_n^z \rangle]/4$. The mean transverse magnetization $\langle \sigma^z \rangle$ and two-point correlation functions can be written as

$$\langle \sigma^z \rangle = -G_0, \quad (3)$$

$$\langle \sigma_m^x \sigma_n^x \rangle = \begin{vmatrix} G_{-1} & G_{-2} & \dots & G_{-R} \\ G_0 & G_{-1} & \dots & G_{-R+1} \\ \vdots & \vdots & \ddots & \vdots \\ G_{R-2} & G_{R-3} & \dots & G_{-1} \end{vmatrix}, \quad (4)$$

$$\langle \sigma_m^y \sigma_n^y \rangle = \begin{vmatrix} G_1 & G_0 & \dots & G_{-R+2} \\ G_2 & G_1 & \dots & G_{-R+3} \\ \vdots & \vdots & \ddots & \vdots \\ G_R & G_{R-1} & \dots & G_1 \end{vmatrix}, \quad (5)$$

$$\langle \sigma_m^z \sigma_n^z \rangle = G_0^2 - G_R G_{-R}, \quad (6)$$

with

$$G_R = -\frac{1}{N} \sum_k \tanh(\beta \varepsilon_k) [\cos(\chi_k R) \cos \theta_k + \sin(\chi_k R) \sin \theta_k], \quad (7)$$

where $R = |m - n|$ represents the distance of spin pairs, $\beta = 1/(k_B T)$, where k_B is the Boltzmann constant, and $\chi_k = \frac{2\pi k}{N} (M = \frac{N-1}{2}, k = -M, -M+1, \dots, M-1, M)$. The $\sin \theta_k = [\alpha \delta \sin(2\chi_k) + \gamma \sin \chi_k]/\varepsilon_k$, and $\cos \theta_k = [\alpha \cos(2\chi_k) + \cos \chi_k - \lambda]/\varepsilon_k$, with the energy spectra ε_k read

$$\varepsilon_k = \pm \{ [\alpha \cos(2\chi_k) + \cos \chi_k - \lambda]^2 + [\alpha \delta \sin(2\chi_k) + \gamma \sin \chi_k]^2 \}^{1/2}. \quad (8)$$

Now we start to analyze the topological characterizations of the extended XY model. The Pauli operators in Eq. (1) can be mapped to the spinless fermion operators by the Jordan-Wigner transformation, and by following Fourier, Bogoliubov transformation, we can obtain the form of the Bogoliubov–de Gennes Hamiltonian as [23]

$$H = \sum_k (c_k^\dagger \quad c_{-k}) \mathcal{H}_k \begin{pmatrix} c_k \\ c_{-k}^\dagger \end{pmatrix}, \quad (9)$$

where $\mathcal{H}_k = \vec{r}(k) \cdot \vec{\sigma}$ with $\vec{r}(k) = [0, Y(k), Z(k)]$ and $\vec{\sigma} = (\sigma^x, \sigma^y, \sigma^z)$. The vector $\vec{r}(k)$ represents a two-dimensional magnetic field, its components can be expressed as

$$Y(k) = \alpha \delta \sin(2\chi_k) + \gamma \sin \chi_k, \\ Z(k) = \alpha \cos(2\chi_k) + \cos \chi_k - \lambda. \quad (10)$$

In the auxiliary two-dimensional y - z plane, we can establish the connection between the TQPTs and the switch of the topological quantities via winding number, which is a fundamental concept in geometric topology, and is equal to the Chern number and the Majorana charge in a generalized quantum spin system [12]. The winding number of a closed loop in the auxiliary y - z plane around the origin point is defined as [11]

$$\mathcal{N} = \frac{1}{2\pi} \oint (Y dZ - Z dY) / |\vec{r}|^2, \quad (11)$$

which is an integer representing the total number of times that the curve travels around the origin point, and we can use it to identify different topological quantum phases in the extended XY model. In addition, we can obtain critical points of different topological quantum phases by solving the corresponding characteristic equations [23,25,27].

B. Quantum Fisher information

We briefly introduce the QFI by a general phase estimation scenario. A quantum system, undergoing unitary transformation, can be described as $\rho_\theta = e^{-iA\theta} \rho e^{iA\theta}$, where θ is the parameter to be estimated and the A is an observable. When we infer the value of θ by use of the parameter estimation approach, the measurement error is unavoidable due to quantum and statistical fluctuations. The precision of estimating θ is restricted by the quantum Cramér-Rao inequality [39,40]

$$\Delta \hat{\theta} \geq \frac{1}{\sqrt{\mu \mathcal{F}(\rho_\theta)}}, \quad (12)$$

where μ is the number of times with the repeated measurement, and $\mathcal{F}(\rho_\theta)$ is defined as the QFI. If ρ is a mixed state, whose orthogonal spectral decomposition can be expressed as $\rho = \sum_m \lambda_m |m\rangle \langle m|$, where λ_m and $|m\rangle$ are the eigenvalues and eigenvectors of the density matrix ρ , respectively, then the specific expression of QFI can be written in the following form [41,42]:

$$\mathcal{F}(\rho, A) = \sum_{m,n} \frac{(\lambda_m - \lambda_n)^2}{2(\lambda_m + \lambda_n)} | \langle m | A | n \rangle |^2. \quad (13)$$

For any bipartite state ρ_{ij} , by means of the local orthonormal observable bases $\{A_\mu\}$ and $\{B_\mu\}$ of two subsystems, the

QFI, encoded in the bipartite system with respect to observables, can be expressed as [42]

$$\mathcal{F} = \sum_{\mu} \mathcal{F}(\rho, A_{\mu} \otimes I + I \otimes B_{\mu}), \quad (14)$$

where the local orthonormal observable bases $\{A_{\mu}\}$ and $\{B_{\mu}\}$, for a general two-spin system, can be chosen as

$$\{A_{\mu}\} = \{B_{\mu}\} = \frac{1}{\sqrt{2}}\{I, \sigma_1, \sigma_2, \sigma_3\}, \quad (15)$$

where σ_i ($i = 1, 2, 3$) are the Pauli matrices. Moreover, the QFI derived from Eq. (14) is independent of the choice of local orthonormal bases, and it implies that the QFI is the intrinsic quantity of the composite system. Consequently, we will study the QFI of the spin pairs in the extended XY model with topological characterizations by this method in the following section.

III. QFI AND TQPTS IN AN EXTENDED XY MODEL

In this section we investigate the connection between the QFI of the spin pairs and the TQPTs of the extended XY chain driven by four physical quantities, including the anisotropy of the nearest-neighbor spins γ , the anisotropy of the next-nearest-neighbor spins δ , the transverse magnetic field λ , and three-spin interaction α . Simultaneously, the impacts of the thermal fluctuations and the distance of the spin pairs on the relation between the QFI and TQPTs are investigated in detail.

First, we can obtain the analytical expression of QFI according to Eqs. (2), (13), (14), and (15), whose special form can be written as

$$\mathcal{F} = \frac{2(\lambda_1 - \lambda_4)^2}{\lambda_1 + \lambda_4} + \frac{2(\lambda_2 - \lambda_4)^2}{\lambda_2 + \lambda_4} + \frac{8(y^-)^2}{\lambda_1 + \lambda_2}, \quad (16)$$

where $\lambda_1 = \frac{1}{2}[u^+ + u^- - \sqrt{(u^+ - u^-)^2 + 4(y^-)^2}]$, $\lambda_2 = \frac{1}{2}[u^+ + u^- + \sqrt{(u^+ - u^-)^2 + 4(y^-)^2}]$, and $\lambda_4 = z + y^+$, which are three out of four eigenvalues of Eq. (2). Consequently, we can investigate the QFI of spin pairs in the extended XY model.

A. The QFI and the TQPTs driven by the anisotropy of the nearest-neighbor spins

The anisotropy parameter γ describes the anisotropy of the nearest-neighbor spins. The values $\gamma = 0$ and $\gamma = 1$ correspond to the isotropic XX model and Ising model, respectively. In the extended XY model, we first study the TQPTs driven by γ , and investigate the critical behaviors of QFI as well as the influences of the thermal fluctuations and the distance of the spin pairs.

We set the parameters of the extended XY model as $N = 1001$, $\alpha = 1$, $\delta = 1$, $\lambda = -0.5$, and change the value of γ . The energy spectra are displayed in Fig. 1(a), which shows two phase transition points. The critical points of the TQPTs can be derived by solving the characteristic equation $\alpha[\xi^2 + (1 - \delta)\xi^{-2}/2] + \xi + (1 - \gamma)\xi^{-1}/2 - \lambda = 0$, where $\xi = \exp(\frac{i2\pi k}{N})$ and $|\xi| = 1$. In the case of $N = 1001$, $\alpha = 1$, $\delta = 1$, and $\lambda = -0.5$, we can obtain the two critical points by numerical solution, which are $\gamma_{c1} \simeq -0.618$ and $\gamma_{c2} \simeq 1.618$ [25]. The trajectories of the winding vectors

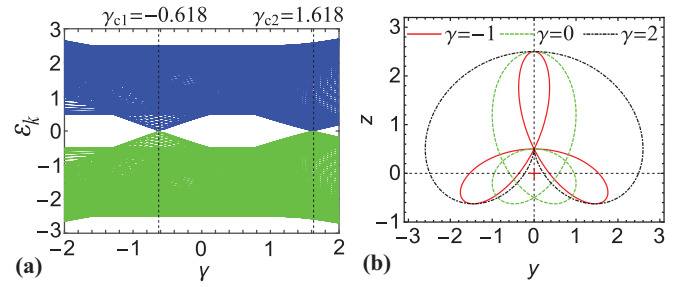


FIG. 1. (a) Energy spectra as a function of γ . (b) Trajectories of the winding vectors in the y - z plane with parameters $\gamma = -1, 0$, and 2 , the winding numbers are $0, 2$, and 0 , respectively. The other parameters are set to $N = 1001$, $\alpha = 1$, $\delta = 1$, and $\lambda = -0.5$.

are plotted in Fig. 1(b) with $\gamma = -1, 0, 2$. The winding numbers can be obtained in the auxiliary y - z plane according to Eq. (11), and it changes from 0 to 2 at γ_{c1} , and from 2 to 0 at γ_{c2} .

Although quantum phase transitions theoretically occur at absolute zero temperature, they can still be observed under a finite temperature, where the system remains dominated by quantum fluctuations, and the thermal fluctuations are not strong enough to excite the ground state. To investigate the impact of thermal fluctuations on the capacity of QFI to detect TQPTs is a significant work on both a theoretical and experimental level. Here we study how the temperature affects the critical behaviors of QFI for the nearest-neighbor spins (i.e., $R = 1$). In Fig. 2 the two-spin QFI and its first derivative as a function of the anisotropy parameter with different temperatures are plotted. It can be seen from Fig. 2(a) that the curves of the QFI with different temperatures almost overlap, and do not have an obvious change at the phase transition points. However, at zero temperature, the divergent behavior of its first derivative can correctly mark the topological phase transition points $\gamma_{c1} \simeq -0.618$ and $\gamma_{c2} \simeq 1.618$ in Fig. 2(b). With the increase of temperature, the divergent behaviors of QFI will become smoother and be replaced by local extrema at the topological phase transition points. It is worth to note that some local extrema drift away from the critical points when we increase the temperature. Therefore, the impact of thermal fluctuations needs to be considered when we use QFI to characterize the TQPTs.

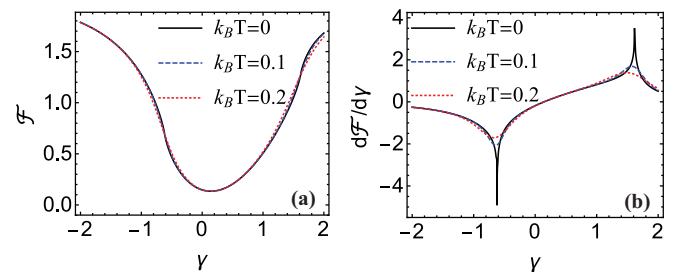


FIG. 2. (a) QFI and (b) its first derivative (with respect to γ) as a function of γ for the nearest-neighbor spins with different temperatures. The other parameters are set to $N = 1001$, $\alpha = 1$, $\delta = 1$, $\lambda = -0.5$, and $R = 1$.

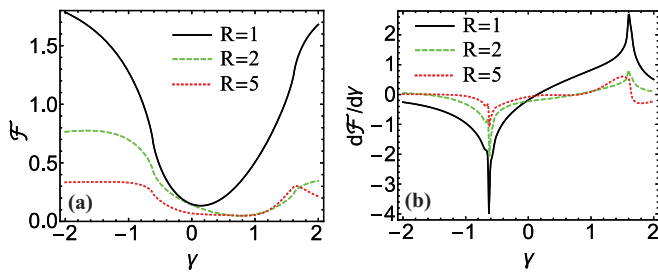


FIG. 3. (a) QFI and (b) its first derivative (with respect to γ) as a function of γ with different site distances at absolute zero temperature. The other parameters are set to $N = 1001$, $\alpha = 1$, $\delta = 1$, and $\lambda = -0.5$.

On the other hand, we also investigate the QFI and its first derivative as a function of the anisotropy parameter with different distances of the spin pairs, and plot them in Fig. 3. It can be seen from Fig. 3(a) that the QFI decreases as the distance increases in most regions of the anisotropy parameter, and does not have a prominent characteristic to mark topological phase transition points for the distance of the spin pairs $R = 1$ and $R = 2$. However, in the case of $R = 5$, the QFI can mark the critical point ($\gamma_{c2} \simeq 1.618$) by the local maximum. In Fig. 3(b), we notice that the divergent behaviors of first derivative for the QFI can correctly characterize the topological phase transition points, but for the case of distance $R = 5$, the first derivative marks the phase transition point ($\gamma_{c2} \simeq 1.618$) by a sharp drop not a divergent behavior or local extremum. In addition, we also find that the peaks of $d\mathcal{F}/d\gamma$ become smaller with increasing R , but the QFI of the long-range spin pairs still mark correctly the TQPTs driven by the anisotropy of the nearest-neighbor spins.

B. The QFI and the TQPTs driven by the anisotropy of the next-nearest-neighbor spins

In this section we study the TQPTs induced by the anisotropy of the next-nearest-neighbor spins and the corresponding critical behaviors of QFI. First, we consider the parameters of the extended XY model (i.e., extended Ising model due to $\gamma = 1$) as $N = 1001$, $\alpha = 1$, $\gamma = 1$, and $\lambda = -0.3$. Then the critical points of TQPTs can be obtained by solving the characteristic equation, which are $\delta_{c1} \simeq -1.2747$ and $\delta_{c2} \simeq 0.5604$ [21]. The energy spectra are displayed in Fig. 4(a), which shows three different topological phases. The

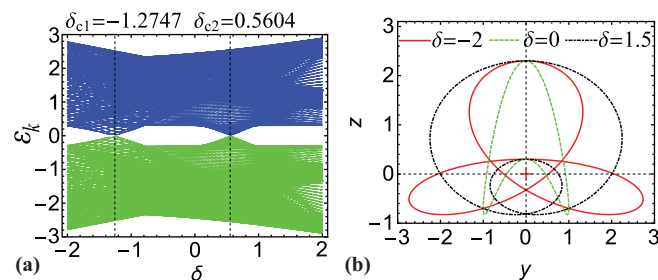


FIG. 4. (a) Energy spectra as a function of δ . (b) Trajectories of the winding vectors in the y - z plane with parameters $\delta = -2, 0$, and 1.5 , the winding numbers are 2, 0, and -2 , respectively. The other parameters are set to $N = 1001$, $\alpha = 1$, $\gamma = 1$, and $\lambda = -0.3$.

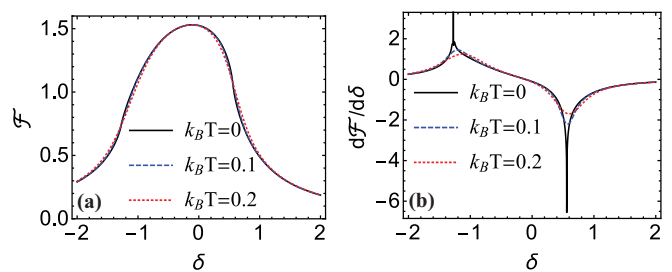


FIG. 5. (a) QFI and (b) its first derivative (with respect to δ) as a function of δ for the nearest-neighbor spins with different temperatures. The other parameters are set to $N = 1001$, $\alpha = 1$, $\gamma = 1$, $\lambda = -0.3$, and $R = 1$.

trajectories of the winding vectors are plotted in Fig. 4(b) with $\delta = -2, 0, 1.5$. The winding numbers can be obtained in the auxiliary y - z plane according to Eq. (11), and it changes from 2 to 0 at δ_{c1} , and from 0 to -2 at δ_{c2} .

For completeness, we also consider the impact of the thermal fluctuations on the critical behaviors of QFI for the nearest-neighbor spins (i.e., $R = 1$). Figure 5 shows the QFI and its first derivative as a function of the anisotropy parameter δ with different temperatures. One can see that the variation curves for QFI versus anisotropy parameter δ with different temperatures almost overlap, and cannot mark any topological phase transition points. However, the divergent behavior of its first derivative at absolute zero temperature can correctly mark the locations of the topological phase transitions at $\delta_{c1} \simeq -1.2747$ and $\delta_{c2} \simeq 0.5604$ in Fig. 5(b). With the increase of temperature, the divergent behaviors of the first derivative will become smoother and be replaced by local extrema at the topological phase transition points. One can notice that these local extrema drift away from the critical points when the temperature increases. Therefore, the impact of thermal fluctuations need to be considered when we study the relationship between the QFI and the TQPTs in a many-body system.

Figure 6 shows the QFI and its first derivative as a function of the anisotropy parameter δ with different site distances of spin pairs. It can be seen from Fig. 6(a) that the QFI decreases as the site distance increases, and the QFI does not mark topological phase transition points for the site distances $R = 1$ and $R = 2$. However, in the case of $R = 5$, the QFI can mark the critical point ($\delta_{c2} \simeq 0.5604$) by the local max-

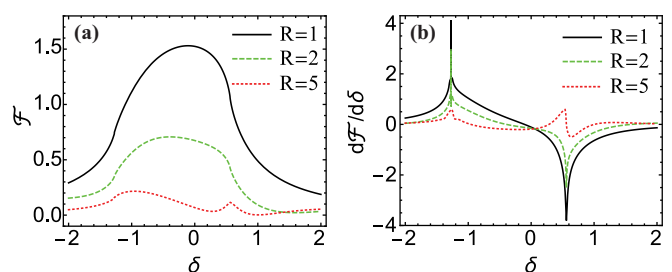


FIG. 6. (a) QFI and (b) its first derivative (with respect to δ) as a function of δ with different site distances at absolute zero temperature. The other parameters are set to $N = 1001$, $\alpha = 1$, $\gamma = 1$, and $\lambda = -0.3$.

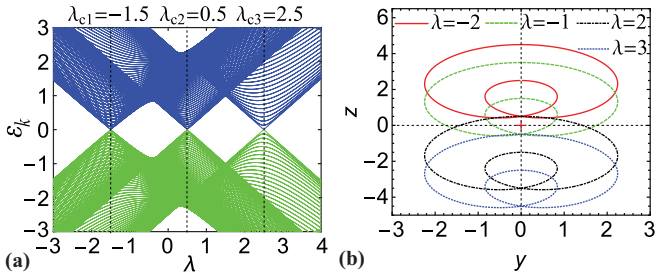


FIG. 7. (a) Energy spectra as a function of λ . (b) Trajectories of the winding vectors in the y - z plane with parameters $\lambda = -2, -1, 2$, and 3 , the winding numbers are $0, 2, 1$, and 0 , respectively. The other parameters are set to $N = 1001$, $\alpha = 1.5$, $\gamma = 1$, and $\delta = 1$.

imum. In Fig. 6(b) one can see that the divergent behaviors of its first derivative can correctly characterize the critical points of TQPTs, but for the case of the distance $R = 5$, its first derivative marks the topological phase transition point ($\delta_{c2} \simeq 0.5604$) by a sharp drop not a divergent behavior or local extremum. We also find that the peaks of their first derivative become smaller with increasing R , but the accuracy of QFI to mark the TQPTs is not influenced by the site distance of spin pairs in an extended Ising model.

C. The QFI and the TQPTs driven by the transverse magnetic field

Now we turn to study the TQPTs induced by the transverse magnetic field and the corresponding critical behaviors of QFI in an extended Ising model (due to $\gamma = 1$ in this section). For given system parameters $\{N = 1001, \alpha = 1.5, \gamma = 1, \delta = 1\}$, we can obtain the topological phase transition points by solving the characteristic equation $1.5\xi^2 + \xi - \lambda = 0$, which are $\lambda_{c1} = -1.5$ for $\xi_1 = \exp[\pm i \arccos(-1/3)]$, $\lambda_{c2} = 0.5$ for $\xi_2 = -1$, and $\lambda_{c3} = 2.5$ for $\xi_3 = 1$ [27]. The energy spectra are displayed in Fig. 7(a), which also indicates that $\lambda_{c1} = -1.5$, $\lambda_{c2} = 0.5$, and $\lambda_{c3} = 2.5$ are the topological phase transition points. The trajectories of the winding vectors in the auxiliary y - z plane are plotted in Fig. 7(b), which shows that with the increase of λ , the winding number changes from 0 to 2 at $\lambda_{c1} = -1.5$, from 2 to 1 at $\lambda_{c2} = 0.5$, and from 1 to 0 at $\lambda_{c3} = 2.5$.

Figure 8 shows the QFI and its first derivative as a function of the transverse magnetic field λ for the nearest-neighbor

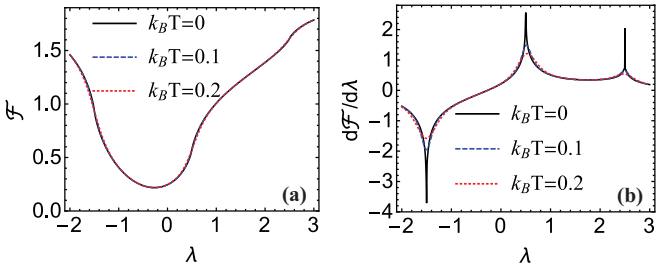


FIG. 8. (a) QFI and (b) its first derivative (with respect to λ) as a function of λ for the nearest-neighbor spins with different temperatures. The other parameters are set to $N = 1001$, $\alpha = 1.5$, $\gamma = 1$, $\delta = 1$, and $R = 1$.

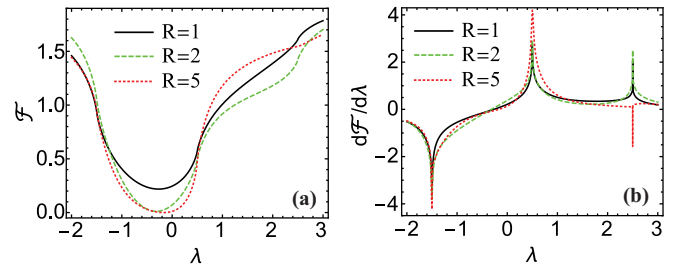


FIG. 9. (a) QFI and (b) its first derivative (with respect to λ) as a function of λ for different site distances at absolute zero temperature. The parameters are set to $N = 1001$, $\alpha = 1.5$, $\gamma = 1$, and $\delta = 1$.

spins with the different temperatures. One can see that the QFI itself cannot mark any phase transition point at the different temperatures. However, the divergent behavior of its first derivative at absolute zero temperature can correctly mark the locations of the topological phase transitions at $\lambda_{c1} = -1.5$, $\lambda_{c2} = 0.5$, and $\lambda_{c3} = 2.5$ in Fig. 8(b). With the increase of temperature, the divergent behaviors of its first derivative of QFI will become smoother and be replaced by local extrema at the topological phase transition points. Therefore, we can conclude that the thermal fluctuations will weaken the corresponding relationship between QFI and TQPTs driven by the transverse magnetic field. Figure 9 shows the QFI and its first derivative as a function of the transverse magnetic field λ for different site distances of spin pairs. In Fig. 9(b) one can see that the divergent behaviors of first derivative of the QFI, for the different site distances of the spin pairs, can correctly characterize the critical points of TQPTs. Remarkably, we find that the peak values of their first derivative become larger with increasing R . We can conclude that the site distance will strengthen the corresponding relation between the QFI and the TQPTs driven by the transverse magnetic field λ .

D. The QFI and the TQPTs driven by the three-spin interaction

The three-spin interaction, as well as multiple spin-exchange model, seems closer to the real situation. Researchers have done extensive researches on the three-spin interaction in experimental and theoretical aspects recently. The conclusions indicate that the three-spin interaction plays a very important role on the physical properties of some quantum concepts in the spin-chain model, such as the QPTs [43], quantum correlations and coherence [20,21,44,45], magnetoelectric and magnetocaloric effect [46,47], and non-Markovianity [48]. Therefore, it is significant for us to study the impact of the three-spin interaction on topological characterization in the extended XY model. We set the parameters of the extended XY model as $N = 1001$, $\gamma = 1$, $\delta = -1$, $\lambda = 1$, and change the value of α . The topological phase transition points can be derived by solving the characteristic equation $\alpha\xi^2 + \xi - 1 = 0$, which are $\alpha_{c1} = (-\sqrt{5} - 1)/2$, $\alpha_{c2} = 0$, $\alpha_{c3} = (\sqrt{5} - 1)/2$, and $\alpha_{c4} = 2$ with $\xi_1 = \exp\{\pm i \arccos[(1 - \sqrt{5})/4]\}$, $\xi_2 = 1$, $\xi_3 = \exp\{\pm i \arccos[(1 + \sqrt{5})/4]\}$, and $\xi_4 = -1$, respectively [25,27]. The energy spectra are displayed in Fig. 10(a), which also proves the four critical points of TQPTs induced by the three-spin interaction. The trajectories

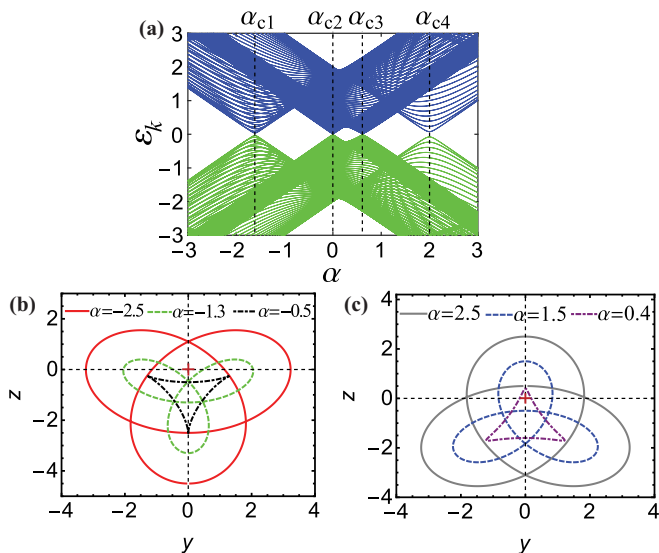


FIG. 10. (a) Energy spectra as a function of α . (b) and (c) Trajectories of the winding vectors in the y - z plane with parameters $\alpha = -2.5, -1.3, -0.5, 0.4, 1.5$, and 2.5 , the winding numbers are 2, 0, 0, 1, -1, and -2, respectively. The other parameters are set to $N = 1001$, $\gamma = 1$, $\delta = -1$, and $\lambda = 1$.

of the winding vectors are plotted in Figs. 10(b) and 10(c) with $\alpha = -2.5, -1.3, -0.5, 0.4, 1.5$, and 2.5 , one can see that the winding numbers in the auxiliary y - z plane change from 2 to 0 at α_{c1} , from 0 to 1 at α_{c2} , from 1 to -1 at α_{c3} , and from -1 to -2 at α_{c4} .

Figure 11 gives the QFI and its first derivative as a function of the three-spin interaction for the nearest-neighbor spins in the extended Ising model with different temperatures. We see that the QFI with different temperatures cannot mark any topological phase transition point. However, the divergent behavior of its first derivative at absolute zero temperature can correctly mark the locations of the TQPTs at $\alpha_{c1} = (-\sqrt{5} - 1)/2$, $\alpha_{c2} = 0$, $\alpha_{c3} = (\sqrt{5} - 1)/2$, and $\alpha_{c4} = 2$ in Fig. 11(b). With the increase of temperature, the divergent behaviors of the first derivative of QFI will become smoother and be replaced by local extrema at the critical points. Moreover, the first derivative of QFI cannot mark the topological phase transition point at $\alpha_{c2} = 0$, and the local extrema drift away from critical points at other topological phase transition

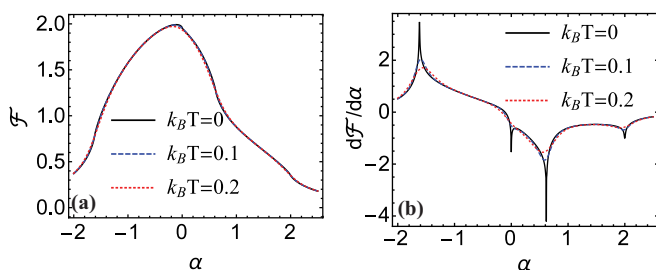


FIG. 11. (a) QFI and (b) its first derivative (with respect to α) as a function of α for the nearest-neighbor spins with different temperatures. The other parameters are set to $N = 1001$, $\gamma = 1$, $\delta = -1$, $\lambda = 1$, and $R = 1$.

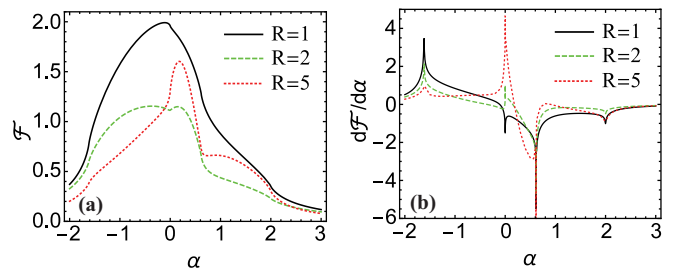


FIG. 12. (a) QFI and (b) its first derivative (with respect to α) as a function of α for different site distances at absolute zero temperature. The other parameters are set to $N = 1001$, $\gamma = 1$, $\delta = -1$, and $\lambda = 1$.

points as a result of the thermal fluctuations. Therefore, the impact of thermal fluctuations need to be considered when we use QFI to characterize the TQPTs induced by three-spin interaction. Figure 12 shows the QFI and its first derivative as a function of the three-spin interaction α for different site distances of spin pairs. It can be seen from Fig. 12(a) that the QFI does not mark topological phase transition points. In Fig. 12(b) one can see that the first derivative of the QFI for long-distance spin pairs can correctly characterize the critical points of TQPTs driven by the three-spin interaction.

As we all know, any quantum detection and estimation incurs measurement error due to various factors such as different quantum states, the imperfection of measurement devices, or the stochasticity of the event in question. The fundamental attainable accuracy in metrology can be obtained by the Cramér-Rao bound. The TQPTs are often accompanied by an abrupt change of systematic energy [such as Figs. 1(a), 4(a), 7(a), and 10(a)] and the quantum resources (quantum correlations and coherence) [20,25]. These changes may eventually affect the measurement error, i.e., the QFI. Our results show that the first derivative of QFI (by the divergent behavior) can characterize correctly TQPTs. It implies that the variation tendency of QFI (with respect to four driven parameters) has an abrupt change due to the TQPTs.

IV. CONCLUSIONS

We have investigated the QFI of spin pairs in an extended XY model with rich topological characterizations. By means of the energy spectra of the ground state and the trajectories of winding vectors (winding number \mathcal{N}) in the auxiliary y - z plane, we systematically studied the topological characterizations of quantum phase transitions driven by the anisotropies of the nearest-neighbor and the next-nearest-neighbor spins, the transverse magnetic field, and the three-spin interaction. Remarkably, we find that the first derivative of QFI can correctly characterize the TQPTs at absolute zero temperature. On the other hand, we also consider the impact of the thermal fluctuations and the site distance of spin pairs on the critical behaviors of QFI and its first derivative. As temperature increases, the divergence of the first derivative of the QFI (with respect to the corresponding driving parameter) becomes smoother and even disappeared, thus the first derivative of QFI can only correctly characterize the critical points of the TQPTs at sufficiently low temperature. However, the

QFI or its first derivative for long-distance spin pairs can still mark the topological phase transition points. In addition, the QFI itself can characterize the TQPTs as the γ and δ are the driven parameters and the site distance $R = 5$. We hope that the properties of the QFI revealed in our work will be useful for experimental studies in the future.

ACKNOWLEDGMENTS

This work was supported by the National Natural Science Foundation of China under Grants No. 61575055, No. 11874132, and No. 11675046. We are thankful to Dr. Jinlei Wu and Dr. Yan Wang for valuable suggestions.

-
- [1] B. Zeng, X. Chen, D. L. Zhou, and X. G. Wen, *Quantum Information Meets Quantum Matter: From Quantum Entanglement to Topological Phases of Many-Body Systems* (Springer Science & Business Media, New York, 2019).
- [2] Y. Xia, D. Qian, D. Hsieh, L. Wray, A. Pal, H. Lin, A. Bansil, D. Grauer, Y. S. Hor, R. J. Cava, and M. Z. Hasan, *Nat. Phys.* **5**, 398 (2009).
- [3] J. Alicea, *Rep. Prog. Phys.* **75**, 076501 (2012).
- [4] S. M. Albrecht, A. P. Higginbotham, M. Madsen, F. Kuemmeth, T. S. Jespersen, J. Nygard, P. Krogstrup, and C. M. Marcus, *Nature (London)* **531**, 206 (2016).
- [5] J. D. Sau, R. M. Lutchyn, S. Tewari, and S. Das Sarma, *Phys. Rev. Lett.* **104**, 040502 (2010).
- [6] J. Alicea, Y. Oreg, G. Refael, F. von Oppen, and M. P. A. Fisher, *Nat. Phys.* **7**, 412 (2011).
- [7] C. V. Kraus, P. Zoller, and M. A. Baranov, *Phys. Rev. Lett.* **111**, 203001 (2013).
- [8] R. S. K. Mong, D. J. Clarke, J. Alicea, N. H. Lindner, P. Fendley, C. Nayak, Y. Oreg, A. Stern, E. Berg, K. Shtengel, and M. P. A. Fisher, *Phys. Rev. X* **4**, 011036 (2014).
- [9] X. Y. Feng, G. M. Zhang, and T. Xiang, *Phys. Rev. Lett.* **98**, 087204 (2007).
- [10] X. L. Qi and S. C. Zhang, *Rev. Mod. Phys.* **83**, 1057 (2011).
- [11] G. Zhang and Z. Song, *Phys. Rev. Lett.* **115**, 177204 (2015).
- [12] G. Zhang, C. Li, and Z. Song, *Sci. Rep.* **7**, 8176 (2017).
- [13] T. Farajollahpour and S. A. Jafari, *Phys. Rev. B* **98**, 085136 (2018).
- [14] T. Mizoguchi and T. Koma, *Phys. Rev. B* **99**, 184418 (2019).
- [15] A. D. King, J. Carrasquilla, J. Raymond, I. Ozfidan, E. Andriyash, A. Berkley, M. Reis, T. Lanting, R. Harris, F. Altomare, K. Boothby, P. I. Bunyk, C. Enderud, A. Fréchet, E. Hoskinson, N. Ladizinsky, T. Oh, G. Poulin-Lamarre, C. Rich, Y. Sato, A. Y. Smirnov, L. J. Swenson, M. H. Volkmann, J. Whittaker, J. Yao, E. Ladizinsky, M. W. Johnson, J. Hilton, and M. H. Amin, *Nature (London)* **560**, 456 (2018).
- [16] W. Cai, J. Han, F. Mei, Y. Xu, Y. Ma, X. Li, H. Wang, Y. P. Song, Z.-Y. Xue, Z.-q. Yin, S. Jia, and L. Sun, *Phys. Rev. Lett.* **123**, 080501 (2019).
- [17] A. Y. Kitaev, *Phys. Usp.* **44**, 131 (2001).
- [18] W. DeGottardi, D. Sen, and S. Vishveshwara, *New J. Phys.* **13**, 065028 (2011).
- [19] L. Zhang, S. P. Kou, and Y. J. Deng, *Phys. Rev. A* **83**, 062113 (2011).
- [20] J. L. Guo and X. Z. Zhang, *Sci. Rep.* **6**, 32634 (2016).
- [21] X. Z. Zhang and J. L. Guo, *Quantum Inf. Process.* **16**, 223 (2017).
- [22] L. Pezzè, M. Gabbriellini, L. Lepori, and A. Smerzi, *Phys. Rev. Lett.* **119**, 250401 (2017).
- [23] Y. R. Zhang, Y. Zeng, H. Fan, J. Q. You, and F. Nori, *Phys. Rev. Lett.* **120**, 250501 (2018).
- [24] N. C. Randeep and N. Surendran, *Phys. Rev. B* **98**, 125136 (2018).
- [25] S. P. Li and Z. H. Sun, *Phys. Rev. A* **98**, 022317 (2018).
- [26] Q. Chen, G. Q. Zhang, J. Q. Cheng, and J. B. Xu, *Quantum Inf. Process.* **18**, 8 (2019).
- [27] Y. K. Wang, Y. R. Zhang, and H. Fan, *Quantum Inf. Process.* **18**, 19 (2019).
- [28] S. L. Braunstein and C. M. Caves, *Phys. Rev. Lett.* **72**, 3439 (1994).
- [29] S. L. Braunstein, C. M. Caves, and G. J. Milburn, *Ann. Phys.* **247**, 135 (1996).
- [30] R. A. Fisher, *Proc. Cambridge Philos. Soc.* **22**, 700 (1925).
- [31] V. Giovannetti, S. Lloyd, and L. Maccone, *Phys. Rev. Lett.* **96**, 010401 (2006).
- [32] S. Boixo, S. T. Flammia, C. M. Caves, and J. M. Geremia, *Phys. Rev. Lett.* **98**, 090401 (2007).
- [33] S. Boixo, A. Datta, M. J. Davis, S. T. Flammia, A. Shaji, and C. M. Caves, *Phys. Rev. Lett.* **101**, 040403 (2008).
- [34] S. M. Roy and S. L. Braunstein, *Phys. Rev. Lett.* **100**, 220501 (2008).
- [35] X. M. Liu, W. W. Cheng, and J. M. Liu, *Sci. Rep.* **6**, 19359 (2016).
- [36] X. M. Liu, Z. Z. Du, and J. M. Liu, *Quantum Inf. Process.* **15**, 1793 (2016).
- [37] Q. Wang and W. G. Wang, *Mod. Phys. Lett. B* **31**, 1750107 (2017).
- [38] B. L. Ye, B. Li, Z. X. Wang, X. Q. Li-Jost, and S. M. Fei, *Sci. China-Phys. Mech. Astron.* **61**, 110312 (2018).
- [39] C. W. Helstrom, *Quantum Detection and Estimation Theory* (Academic, New York, 1976).
- [40] A. S. Holevo, *Probabilistic and Statistical Aspects of Quantum Theory* (North-Holland, Amsterdam, 1982).
- [41] S. L. Luo, *Proc. Am. Math. Soc.* **132**, 885 (2004).
- [42] N. Li and S. L. Luo, *Phys. Rev. A* **88**, 014301 (2013).
- [43] W. L. You, Y. C. Qiu, and A. M. Oleś, *Phys. Rev. B* **93**, 214417 (2016).
- [44] J. Yang and Y. X. Huang, *Quantum Inf. Process.* **16**, 281 (2017).
- [45] Y. T. Sha, Y. Wang, Z. H. Sun, and X. W. Hou, *Ann. Phys.* **392**, 229 (2018).
- [46] O. Menchshyn, V. Ohanyan, T. Verkholyak, T. Krokhmal'skii, and O. Derzhko, *Phys. Rev. B* **92**, 184427 (2015).
- [47] J. Sznajd, *Phys. Rev. B* **97**, 214410 (2018).
- [48] M. Mahmoudi, S. Mahdaviifar, T. M. A. Zadeh, and M. R. Soltani, *Phys. Rev. A* **95**, 012336 (2017).